Baroclinic annular variability in the Northern Hemisphere

David W. J. Thompson and Ying Li

Department of Atmospheric Science, Colorado State University

Fort Collins, CO. USA

Submitted to Journal of Atmospheric Sciences

April 2014

Abstract

Large-scale variability in the Northern Hemisphere (NH) circulation can be viewed in the context of three primary types of structures: 1) teleconnection patterns; 2) a barotropic annular mode; and 3) a baroclinic annular mode. The barotropic annular mode corresponds to the northern annular mode (NAM) and has been examined extensively in previous research. Here we examine the spatial structure and time dependent behavior of the NH baroclinic annular mode (NBAM).

The NAM and NBAM play very different roles in driving large-scale variability in the NH circulation. The NAM emerges as the leading principal component (PC) time series of the *zonal-mean* kinetic energy. It dominates the variance in the wave fluxes of momentum, projects weakly onto the eddy kinetic energy and wave fluxes of heat, and can be modeled as Gaussian red noise with a timescale of ~10 days. In contrast, the NBAM emerges as the leading PC time series of the *eddy* kinetic energy. It is most clearly identified when the planetary-scale waves are filtered from the data, dominates the variance in the synoptic-scale eddy kinetic energy and wave fluxes of heat, and has a relatively weak signature in the zonal-mean kinetic energy and the wave fluxes of momentum. Interestingly, the NBM is marked by enhanced spectral power on timescales of ~20-25 days.

The NBAM is remarkably similar to its Southern Hemisphere counterpart, despite the pronounced interhemispheric differences in orography and land/sea contrasts. The annular scale of the NBAM is consistent with the weak but significant correlations between synoptic-scale eddy activity over the Atlantic and Pacific sectors of the NH.

1. Introduction

Large scale variability in the extratropical circulation is often examined in the context of two primary classes of structures: “teleconnection patterns” and “annular modes”.

Teleconnection patterns are generally defined on the basis of significant negative correlations between widely separated points in the geopotential height field (e.g., Wallace and Gutzler 1981). By construction, they explain large fractions of the geopotential height and wind variance within specific regions of the hemisphere. In contrast, annular modes are typically defined as the leading empirical orthogonal functions of the hemispheric-scale geopotential height and/or zonal wind fields (e.g., Kidson 1988; Hartmann and Lo 1998; Thompson and Wallace 2000). They do not necessarily account for large fractions of the variance in the circulation within specific sectors of the hemisphere. But by construction, they account for large fractions of the variance integrated over the entire hemisphere.

Teleconnection patterns frequently have a notable zonally *asymmetric* component. For example, the Pacific-North America pattern is characterized by wavelike anomalies in the geopotential height field that stretch along a great circle route from the central north Pacific to eastern North America (Wallace and Gutzler 1981; Quadrelli and Wallace 2004); the North Atlantic Oscillation is characterized by north-south fluctuations in the geopotential height field that have largest amplitude in the North Atlantic sector (e.g., Wallace and Gutzler 1981; Hurrell 1995). In contrast, the annular modes have a pronounced zonally *symmetric* component. Both the Northern and Southern Hemisphere annular modes (the NAM and SAM) are characterized by barotropic fluctuations in the geopotential height field that exhibit a high degree of

longitudinal symmetry. The NAM may be viewed as the hemispheric expression of the North Atlantic Oscillation teleconnection pattern (Wallace 2000).

In recent work (Thompson and Woodworth 2014; hereafter TW), we have argued that large scale variability in the extratropical flow of the Southern Hemisphere (SH) can be examined in the context of a third type of structure: a *baroclinic* annular mode. The key results of TW are the following:

1) The SAM is the leading pattern of variability in the SH *zonal-mean kinetic energy*, and it may be viewed as a *barotropic* annular mode. It explains large fractions of the variance in the wave fluxes of momentum, but has a very weak projection onto the eddy fluxes of heat and the eddy kinetic energy.
2) In contrast, the leading pattern of variability in the SH *eddy kinetic energy* may be viewed as a *baroclinic* annular mode. Like the SAM, the southern baroclinic annular mode has a distinct zonally symmetric component. But unlike the SAM, it projects strongly onto the eddy fluxes of heat, and only weakly onto the zonal-mean kinetic energy and eddy fluxes of momentum.
3) The SAM and its baroclinic counterpart play very different roles in SH climate variability. They have contrasting roles in the extratropical energy cycle. They have very different projections on surface climate. And notably, they have very different signatures in the frequency domain: the SAM can be modeled as Gaussian red noise with a timescale of ~10 days (Hartmann and Lo 1998; Lorenz and Hartmann 2001); the southern baroclinic annular mode exhibits marked variability on ~20-30 timescales (TW; Thompson and Barnes 2014).

The purpose of this paper is to extend the analyses of TW to the Northern Hemisphere (NH). We will demonstrate that the NH circulation exhibits a baroclinic annular mode that is very similar to its SH counterpart despite the notable interhemispheric differences in orography and land-sea contrasts. In Section 3, we develop a procedure for identifying baroclinic annular variability in the NH. In Section 4, we investigate the signature of the NH baroclinic annular mode in the zonal-mean circulation, and contrast it to the NH barotropic annular mode (the NAM). In Section 5, we investigate the "annularity" of NH baroclinic annular mode and the inferred teleconnectivity between eddy activity in the North Atlantic and North Pacific sectors. In Section 6, we examine the spectral characteristics of the NH baroclinic annular mode. Conclusions are provided in Section 7.

2. Data/methods

All analyses are based on the European Centre for Medium-Range Weather Forecasts Interim reanalysis data set (ERA-Interim; Dee et al. 2011). The reanalyses output are available on a 1.25° x 1.25° mesh and at 4 *x* daily resolution. The results are based on daily-mean versions of the data for the period 1979-2011. Daily mean precipitation is calculated by averaging total precipitation at 00 and 12UTC at forecast steps of 6 and 12 hours. Anomalies are formed by subtracting the long-term mean seasonal cycle from the data at all time steps.

Throughout the study, brackets denote zonal-mean quantities and * departures from the zonal-mean. The zonal-mean eddy kinetic energy is defined as $\frac{1}{2}[u^{*2} + v^{*2}]$; the zonal-mean eddy fluxes of momentum as $[u^* v^*]$; and the zonal-mean eddy fluxes of heat

as $[v^*T^*]$. Eddy fluxes are calculated at 4 *x* daily resolution and averaged to form daily mean versions of the fluxes.

In cases where we use empirical orthogonal function/principal component (EOF/PC) analyses, the data are weighted by the square root of the cosine of latitude and the mass represented by each vertical level in the ERA-Interim before calculating the covariance matrix of the data.

As discussed in Section 3, the wind data used to identify baroclinic annular variability are spatially filtered to remove the contributions of planetary-scale eddies to the eddy kinetic energy. Planetary scale eddies are defined here as variations on spatial scales of zonal wavenumbers 1-3; synoptic scale eddies as variations on spatial scales of zonal wavenumbers 4 and higher.

The statistical significance of all correlations is assessed using the *t*-statistic, where the effective number of degrees of freedom (N^*) is estimated as:

$$N^* = N\frac{1-r_1r_2}{1+r_1r_2} \qquad (1)$$

where N is the number of time steps used in the correlations, and r_1 and r_2 are the lag-one autocorrelations of the time series being correlated.

Power spectra for time series that span all calendar days are found by: 1) Calculating the spectra for subsets of the time series that are 500 days in length with 250 days overlap between adjacent subsets. Split-cosine-bell tapering is applied to 5% of the data on each end of the subset time series; 2) Averaging the power spectra over all subsets of the time series; and 3) Applying a 3 point running mean to the resulting mean power spectrum. Power spectra for time series limited to the warm and cold seasons are based

on subsets that are 183 days in length for the warm season (April-September) and 182 days in length for the cold season (October-March) with no overlap between subsets.

3. Defining baroclinic annular variability in the Northern Hemisphere

In this section, we develop an index for characterizing baroclinic annular variability in the NH. Throughout the study, the southern and northern *barotropic* annular modes are denoted as the SAM and NAM, respectively, whereas the southern and northern *baroclinic* annular modes are denoted as the SBAM and NBAM, respectively.

The left column in Figure 1 reviews the latitude/lag structure of the southern baroclinic annular mode (the SBAM) in two key fields: the zonal-mean eddy fluxes of heat at 850 hPa and the eddy kinetic energy at 300 hPa. As in TW, the SBAM is defined as the leading PC time series of the zonal-mean eddy kinetic energy for all levels and latitudes within the domain 1000-200 hPa and 20-70°S. By definition, the "positive polarity" of the SBAM is defined as periods when the hemispheric mean eddy kinetic energy is anomalously positive, and vice versa.

Figure 1a shows the unfiltered, zonal mean fields of the eddy fluxes of heat at 850 hPa (shading) and the eddy kinetic energy at 300 hPa (contours) regressed onto the SBAM index as a function of lag and latitude. The figure is identical to Figure 3b from TW, but is calculated using a slightly different time period. As noted in that study, the positive polarity of the SBAM is associated with poleward eddy heat flux anomalies and positive eddy kinetic energy anomalies that span much of the SH middle latitudes. The heat flux anomalies precede the eddy kinetic energy anomalies by ~1-2 days, consistent with the time lag between the generation of wave activity in the lower troposphere and the generation of eddy kinetic energy aloft.

Figures 1c and 1e show the contributions of the synoptic and planetary scale waves to the regressions in the top panel (synoptic and planetary scale waves are defined in Section 2). As evidenced in the left column of Fig. 1, variations in the SBAM are associated almost entirely with eddies on synoptic spatial scales. The dominant role of synoptic scale eddies in variations of the SBAM is consistent with: 1) the relatively weak amplitudes of planetary-scale waves in the SH and 2) the notion that the SBAM owes its existence to two-way feedbacks between the baroclinicity and the eddy fluxes of heat by synoptic-scale waves (Thompson and Barnes 2014).

The right column in Figure 1 shows analogous results calculated for the NH. In all three panels, the regressions are based on the leading PC time series of the zonal-mean eddy kinetic energy for all levels and latitudes within the domain 1000-200 hPa and 20-70°N. As in the SH, the leading PC of NH eddy kinetic energy is marked by same sign fluctuations in both the eddy kinetic energy and eddy fluxes of heat that span much of the midlatitudes (Fig. 1b). However, unlike the SH, the anomalies have a relatively complicated spatial structure, and derive in roughly equal parts from synoptic and planetary scale eddies (Figs. 1d and 1f). Hence, the leading pattern of variability in the NH eddy kinetic energy field includes a notable contribution from the planetary scale eddies that is not reflected in association with the SBAM.

To the extent that baroclinic annular variability reflects the dynamics of baroclinic waves, it follows that a physically meaningful index of baroclinic annular variability should isolate the variance in the eddy kinetic field associated with synoptic-scale eddies. Filtering the eddy kinetic energy field to isolate the variance associated with synoptic-scale eddies is not necessary in the SH, where the planetary-scale waves have relatively weak amplitude. But as evidenced in Fig. 1, it is essential in the NH, where the

planetary scale waves make a prominent contribution to the leading EOF of the eddy kinetic energy. For this reason, we will define the time series of the northern baroclinic annular mode (the NBAM) as the leading PC time series of the eddy kinetic energy associated with wavenumbers 4 and higher. As done for the SH, the PC time series is calculated for all levels and latitudes within the domain 1000-200 hPa and 20-70°N. The patterns associated with the resulting NBAM index are explored in the following sections.

4. Structure of the NAM and NBAM in the zonal-mean circulation

Figures 2-5 compare the structures of the NAM and NBAM in the extratropical zonal-mean circulation. The NAM index is defined as the leading PC time series of the anomalous daily-mean, zonal-mean zonal wind for all levels and latitudes in the domain 1000-200 hPa and 20-70°N. As noted in Section 3, the NBAM index is defined as the leading PC time series of the eddy kinetic energy associated with zonal wavenumbers 4 and higher. The NBAM index explains 43% of the variance in NH synoptic-scale eddy kinetic energy, and both the NAM and NBAM indices are statistically distinct from the second PCs of their respective fields (the variances explained by all PCs considered in this study are listed in Table 1). The positive polarity of the NBAM is defined as periods when the hemispheric mean eddy kinetic energy is anomalously positive, and vice versa. The positive polarity of the NAM is defined as periods when the zonal flow ~55°N is anomalous westerly, and vice versa. Unless otherwise noted, the fields regressed on the NBAM and NAM indices are *not* filtered.

The NAM and NBAM indices are only weakly correlated at all lags between -20 to + 20 days (not shown) and in 10 day low-pass data (Table 2). Roughly 98% of the

variance in the NAM on timescales longer than 10 days is independent of variability in the NBAM.

a. Reviewing the signature of the NAM in the zonal-mean tropospheric circulation

The left column in Fig. 2 reviews the latitude/height profiles of the NAM. As noted extensively in previous work (e.g., Thompson and Wallace 2000; Limpasuvan and Hartmann 2000), the NAM is marked by meridionally banded anomalies in the zonal-mean zonal flow, with primary centers of action located ~30°N and ~55°N (Fig. 2a). The regressions in Fig. 2a also indicate a third center of action in the zonal-flow near 75°N. The center of action near 75°N is restricted to the region to the north of Iceland (not shown), and is not evident in regressions based on the leading PC of the monthly-mean sea-level pressure (Thompson and Wallace 2000) or zonal wind (Lorenz and Hartmann 2003). Likewise, it is much weaker when the time series used to generate Fig. 2a are 30 day low pass filtered. Hence the center of action near 75°N is uniquely linked to NAM-like variability on submonthly timescales. A more detailed analysis of the subpolar center of action in the NAM is left for a future study. For the purpose of this study, it is worth emphasizing that the NAM index used here is very similar to that used in other studies (e.g., the correlation coefficient between monthly-mean values of the NAM index used here and the leading PC time series of the monthly-mean sea-level pressure field 20°-70°N is r=0.87).

As also noted in previous work, the NAM is associated with: 1) poleward momentum fluxes centered near the tropopause ~45°N (shading in Fig. 2a; Limpasuvan and Hartmann 2000; Lorenz and Hartmann 2003); 2) negative temperature anomalies at subpolar latitudes juxtaposed against warm temperature anomalies at middle

latitudes (shading in Figure 2c; Thompson and Wallace 2000); and 3) paired meridional overturning cells with rising motion at subpolar and tropical latitudes juxtaposed against sinking motion between about 30°-40°N (contours in Fig. 2c). The momentum flux anomalies precede the zonal-wind anomalies by several days, consistent with forcing of the zonal-mean flow by the advection of momentum by the eddies (Fig. 3a; Lorenz and Hartmann 2003). The temperature anomalies associated with the NAM are consistent with adiabatic expansion and compression driven by the attendant changes in vertical motion. The vertical motion anomalies, in turn, are consistent with forcing by the momentum fluxes aloft (Thompson and Wallace 2000). Note that the mass streamfunction has very small amplitude at high latitudes in part due to the relatively small area represented by the polar cap (Fig. 2c).

The signatures of the NAM in the zonal wind and eddy fluxes of momentum discussed above are consistent with north-south fluctuations in the extratropical jet (Lorenz and Hartmann 2003). The signatures of the NAM in the eddy kinetic energy and eddy heat flux anomalies are more difficult to interpret (Fig. 2e). To the extent that the heat fluxes and eddy kinetic energy follow vacillations in the jet, the positive polarity of the NAM should be accompanied not only by anomalously poleward momentum fluxes in the upper troposphere near 45°N, but also by increases in the eddy fluxes of heat and eddy kinetic energy near 55°N and decreases near 30°N. Neither feature is clearly apparent in Fig. 2e. As is the case for the SAM (TW), the signature of the NAM in the eddy fluxes of heat is both weak and amorphous throughout most of the midlatitudes (Fig. 2e).

The signature of the NAM in the eddy fluxes of heat and momentum is reviewed further in the left column of Fig. 4. Figure 4a shows the unfiltered wave fluxes of

momentum (contours; reproduced from shading in Fig. 3a) and heat (shading) regressed on the NAM index as a function of lag and latitude. Figures 4c and 4e show the components of the regressions that are due to synoptic (wavenumbers 4 and higher) and planetary-scale (wavenumbers 1-3) waves, respectively. Note that in contrast to the diagnostics presented in DeWeaver and Nigam (2000), Feldstein (2003), and Lorenz and Hartmann (2003), the wave fluxes in Fig. 4 are spatially rather than time filtered.

As evidenced in Figs. 4c and 4e, the preponderance of the eddy momentum flux anomalies associated with the NAM are due to variations in synoptic-scale waves. In contrast, a large fraction of the eddy heat flux anomalies associated with the NAM are due to variations in the planetary-scale waves (Fig. 4e), particularly the meridional dipole in eddy heat flux anomalies centered around lag 0. The most pronounced signature of the NAM in the synoptic-scale wave fluxes of heat is found at positive lag near 50°N (Fig. 4c), and is consistent with the influence of the momentum fluxes aloft on lower tropospheric baroclinicity (Lorenz and Hartmann 2003).

b. The signature of the NBAM in the zonal-mean tropospheric circulation

The structure of the NBAM in the extratropical circulation is shown in the right columns of Figs. 2-4. In contrast to the NAM but like its SH counterpart (TW), the NBAM has a weak signature in the zonal-mean zonal wind and wave fluxes of momentum but a pronounced signature in the zonal-mean eddy kinetic energy and wave fluxes of heat (Figs. 2b and 2f). The NBAM is hence associated with hemispheric scale fluctuations in both the generation of eddies in the lower troposphere (as inferred by the vertical gradient in the eddy fluxes of heat) and their amplitudes aloft (as inferred by the eddy kinetic energy). The eddy heat flux anomalies precede the eddy kinetic energy

anomalies by ~1-2 days, consistent with the generation of upper tropospheric eddy kinetic energy by developing baroclinic waves in the free troposphere (Fig. 3b).

Also like its SH counterpart (TW), the NBAM is marked by warm temperature anomalies at middle latitudes (shading in Fig. 2d) that are consistent with warming by the convergence of the wave fluxes of heat there (shading in Fig. 2f). In contrast to the NAM, the changes in vertical motion are thermally driven, i.e., the midlatitude warming is overlaid by upwards rather than downwards motion (contours in Fig 2d).

In part by construction, the anomalous eddy fluxes of heat and momentum associated with the NBAM are dominated by synoptic scale eddies (right column in Fig. 4). Consistent with the barotropic decay stage of baroclinic waves (Simmons and Hoskins 1978), the NBAM is marked by positive anomalies in the wave fluxes of momentum that lag and lie slightly equatorward of the positive anomalies in the wave fluxes of heat (Fig. 4d).

c. Summarizing the differences between the NAM and NBAM

As is the case in the SH, the barotropic (the NAM) and baroclinic (the NBAM) northern annular modes have very different signatures in the extratropical circulation. The NAM emerges as the leading PC of the zonal-mean kinetic energy (Table 2). It is driven by the wave fluxes of momentum (Fig. 3a), and has a weak secondary signature in the synoptic-scale wave fluxes of heat that is consistent with the influence of the momentum fluxes on tropospheric baroclinicity (Fig. 4c). The NAM hence explains a large fraction of the variance in the zonal-mean zonal wind and eddy fluxes of momentum (left panels in Fig. 5; solid lines), but a relatively small fraction of the

285 variance in the zonal-mean eddy kinetic energy and eddy fluxes of heat (left panels in
286 Fig. 5; dashed lines).

287 In contrast, the NBAM emerges as the leading EOF of the eddy kinetic energy. It
288 is driven by the wave fluxes of heat (Fig. 3b), and has a secondary signature in the wave
289 fluxes of momentum that is consistent with the baroclinic wave lifecycle (Fig. 4d). The
290 NBAM hence explains a notable fraction of the variance in the zonal-mean eddy kinetic
291 energy and eddy fluxes of heat (right panels in Fig. 5; dashed lines), but a very small
292 fraction of the variance in the zonal-mean zonal wind and eddy fluxes of momentum
293 (right panels in Fig. 5; solid lines). The NBAM explains a smaller fraction of the variance
294 in the eddy kinetic energy than the NAM does in the zonal-mean kinetic energy (bottom
295 panels).

296 The results shown in this section are based on data for all calendar months. The
297 NBAM also emerges as the leading PC of synoptic-scale eddy kinetic energy in analyses
298 performed separately for the warm and cold season months. For example, the
299 correlations between 1) warm season (April-September) segments of the NBAM index
300 and 2) the leading PC of warm season synoptic-scale eddy kinetic energy is r~0.99. As is
301 the case for the NAM (Thompson and Wallace 2000), the primary difference in the
302 NBAM between the winter and summer seasons is that its amplitude peaks during the
303 cold season months.

304 In the following section we will assess the "annularity" of the NBAM and the
305 inferred linkages between synoptic eddy activity over the two primary NH stormtrack
306 regions.

307

308

5. The annularity of the NBAM / linkages between the stormtracks

The robust signature of the NBAM in the zonal-mean circulation suggests that it exhibits a high degree of annularity. In this section, we examine to what extent the NBAM reflects: 1) the dominant pattern of variability in the longitudinally-varying circulation; and 2) coordinated variability in synoptic activity between the two major NH storm track regions. The "annularity" of barotropic annular modes – including the NAM - has been discussed at-length in the literature (e.g., Wallace 2000; Gerber and Vallis 2005) and will be examined only briefly here.

a. The leading patterns of variability in the longitudinally-varying circulation

Figure 6 shows the zonally-varying, unfiltered eddy-kinetic energy at the 300 hPa level regressed onto the NBAM index. The resulting pattern suggests that the NBAM is associated with variations in the amplitude of synoptic-scale waves in both the North Pacific and North Atlantic stormtracks. Over the Pacific sector, it is marked by maxima over the Kuroshio extension region and the central North Pacific. Over the Atlantic sector, it is characterized by maxima over the Gulf Stream extension region and the central North Atlantic to the west of Spain.

To what extent does the hemispheric scale structure of the NBAM emerge from PC analyses of the longitudinally varying flow? Figure 7c shows the correlations between a) the leading PCs of the longitudinally varying synoptic-scale eddy kinetic energy calculated as a function of latitude; and b) the NBAM index. Figure 7d shows the corresponding variances explained by the first two PCs of the longitudinally varying synoptic-scale eddy kinetic energy as a function of latitude, where the error bars correspond to the criterion outlined in North et al. (1981). For example, the leading PC

of the longitudinally varying synoptic-scale eddy kinetic energy along 50°N is well separated from the second PC at 50°N (Fig. 7d), and is correlated with the NBAM index at a level of r~0.8 (Fig. 7c). Figures 7a and 7b show the corresponding results for the zonal-mean zonal wind field and the NAM index.

The leading PCs of the longitudinally varying synoptic-scale eddy kinetic energy field are highly correlated with the NBAM index throughout middle latitudes (right panels in Fig. 7). Likewise, the leading PCs of the longitudinally varying zonal wind field are strongly correlated with the NAM index time series at latitudes that lie within the primary centers of action of the NAM (left panels in Fig. 7). Hence, the NAM and NBAM emerge as the leading EOFs of both the zonal-mean and zonally varying components of the zonal wind and eddy-kinetic energy fields, respectively.

b. Connections between the stormtracks

The annularity of the NBAM implies a level of teleconnectivity between the amplitude of synoptic-scale eddy kinetic energy in the North Pacific and Atlantic stormtracks. Several studies have argued that variations in upper tropospheric baroclinic activity in the two stormtracks are significantly correlated (e.g., Chang and Fu 2002; Chang 2004; Li and Lau 2012). But others have noted that the correlations between the stormtracks are very weak (Wettstein and Wallace 2010). The correlations between synoptic-scale eddy kinetic energy in the two stormtracks are investigated further below.

First, we examine to what extent the structure of the NBAM emerges from analyses of the circulation over the North Atlantic and North Pacific sectors of the hemisphere. The results in Fig. 8 are identical to those shown in the right column of Fig.

2, but are derived from analyses restricted to 70°W-110°E (the North Atlantic sector) and 110°E-70°W (the North Pacific sector). For example: The $NBAM_{Atlantic}$ index is defined as the leading PC of the synoptic-scale eddy-kinetic energy from 1000-200 hPa averaged 70°W-110°E, and the results in the left column of Fig. 8 show unfiltered data averaged 70°W-110°E regressed on standardized values of the $NBAM_{Atlantic}$ index. The right column shows analogous results calculated for the North Pacific sector.

The key result in Fig. 8 is that the leading patterns of variability in the amplitude of synoptic-scale eddy activity in the Atlantic and Pacific sectors of the NH both bear strong resemblance to the NBAM. Both are marked by a monopole in the eddy fluxes of heat and eddy kinetic energy centered ~40-45°N (Figs. 8e and 8f); both exhibit positive temperature anomalies that peak ~400hPa near 50°N (Figs. 8c and 8d); and both have a relatively weak signature in the zonal wind field (Figs. 8a and 8b; the momentum flux anomalies associated with the $NBAM_{Atlantic}$ index are shifted slightly equatorward of their Pacific counterparts).

The $NBAM_{Atlantic}$ and $NBAM_{Pacific}$ indices are correlated with the NBAM index at levels of r=0.77 and r=0.79. Hence they contribute roughly equally to variations in the NBAM index. The $NBAM_{Atlantic}$ and $NBAM_{Pacific}$ indices are also significantly linked to each other. Figure 9 shows the correlations between the $NBAM_{Atlantic}$ and $NBAM_{Pacific}$ indices as a function of lag. The leading patterns of synoptic-scale eddy kinetic energy over the North Pacific sector and North Atlantic sectors are significantly linked to each other, particularly when the North Pacific sector leads the North Atlantic sector by ~3-4 days. The correlations between the two sectors are most pronounced during the cold season months (not shown).

The linkages between eddy kinetic energy in the two storm track regions is further evidenced in the lag regressions of (unfiltered) eddy-kinetic energy at the 300 hPa level onto the $NBAM_{Pacific}$ index. At lag 0 (Fig. 10a), the eddy kinetic energy anomalies associated with the $NBAM_{Pacific}$ index have large amplitude over the Pacific sector but do not project onto eddy kinetic energy over the North Atlantic sector. At successive lags, the eddy kinetic anomalies not only decay over the Pacific sector, but appear to propagate/advect downstream towards the North Atlantic sector in a manner consistent with that shown in Chang and Li (1999) and Li and Lau (2012). Roughly ~3-4 days after peak amplitude in the $NBAM_{Pacific}$ index (panels d and e), the North Atlantic stormtrack is marked by positive anomalies in eddy kinetic energy centered over the Gulf Stream extension region. The linkages between eddy kinetic energy in the Pacific sector and over the Gulf Stream extension region ~3-4 days later are statistically significant at the 99% confidence level (Figs. 10d, 10e and 11). The downstream advection of eddy-kinetic energy anomalies from the Atlantic to the Pacific sector is much less clear (not shown).

The results shown in Figs. 9-11 confirm that the linkages between the stormtracks are weak (Wettstein and Wallace 2010). However, consistent with Chang (2004) and Li and Lau (2012), they also suggest that the linkages are significant, particularly when the Pacific stormtrack leads the Atlantic stormtrack by several days. The weak but significant "seeding" of eddy kinetic energy from the North Pacific to North Atlantic storm tracks is seemingly large enough to give rise to a zonally symmetric leading PC of the hemispheric eddy kinetic energy field.

6. Quasi-periodic behavior in the NBAM

The southern baroclinic annular mode exhibits quasi-periodic variability on timescales of ~20-30 days (TW). The quasi-periodic behavior in the SBAM is consistent with two-way feedbacks between the extratropical baroclinicity and the eddy fluxes of heat by baroclinic waves, and extends to large-scale averages of eddy kinetic energy, the eddy fluxes of heat, and precipitation (Thompson and Barnes 2014). Below we investigate to what extent analogous quasi-periodic behavior is evident in association with the NBAM.

The top panel in Figure 12 shows the spectrum of the NBAM index calculated for data for all calendar months (details of the calculation are provided in Section 2). The NBAM index time series exhibits enhanced spectral power centered around ~25 days (~0.04 cpd). The peak in the spectrum is weaker than the corresponding peak in the SBAM (TW, c.f. Fig. 12), but is clearly reproducible in subsets of the data (Fig. 13a and 13b). Interestingly, the spectral peak in the NBAM index derives primarily from the summer season, as evidenced in the middle and lower panels of Fig. 12 (the differences in spectral resolutions between the year-round and seasonal results are due to the subset lengths used in the calculations; Section 2). The wintertime spectrum exhibits enhanced power in the ~20-25 day range, but the spectral peak is much weaker than its summertime counterpart. Both the pronounced spectral peak during summer and the lack of a robust peak during winter are reproducible in both halves of the data record (Fig. 13 middle and bottom panels). The lack of a robust peak during the cold season is consistent with Ambaum and Novak (2013), who did not find evidence of statistically significant periodicity in the North Atlantic stormtrack during the winter season.

The spectral peak in the NBAM during the warm season months extends to various indices of synoptic eddy activity. It is apparent in the spectrum of the hemispheric-mean synoptic-scale eddy kinetic energy at 300 hPa (Fig. 14a). It is apparent in the spectrum of the hemispheric-mean eddy fluxes of heat by synoptic-scale eddies (Fig. 14b). And like its SH analogue, it extends to hemispheric-mean precipitation, albeit the peak in precipitation is less pronounced than it is in the eddy fluxes of heat (Fig. 14c). The spectral peak in the NBAM is examined in more detail in a companion paper (Thompson and Barnes 2015).

7. Concluding remarks

Figure 15 compares the structure of the NBAM with its SH counterpart. The two patterns are remarkably similar. Both are characterized by hemispheric-scale monopoles in the eddy kinetic energy and eddy fluxes of heat (bottom panels). Both have very weak signatures in the wave fluxes of momentum and the zonal-mean zonal flow (top panels). And both are associated with changes in vertical motion and temperature that are consistent with the circulation response to the anomalous fluxes of heat (middle panels, i.e., the regions poleward of the maximum heat flux anomalies are marked by anomalously warm conditions and anomalous rising motion).

The NBAM is also reminiscent of the leading patterns of stormtrack variability identified in previous work. Large-scale “pulsation” of eddy activity also emerges in PC analyses of: 1) the variance of the 10 day high-pass filtered upper tropospheric meridional wind (Wettstein and Wallace 2010) and 2) the rms 2.5-6 day band-pass filtered middle tropospheric geopotential height field (Lau 1988). A key distinction between the NBAM and the modes of pulsing stormtrack activity identified in previous

studies lies in their zonal scales. Wettstein and Wallace (2010) note that the linkages between variability in the North Pacific and North Atlantic stormtracks are very weak, and thus focus primarily on patterns of stormtrack activity within the two ocean basins. The results shown here suggest that the linkages between eddy activity in the Pacific and Atlantic stormtrack regions are statistically significant and are seemingly large enough to give rise to a hemispheric-scale leading EOF of stormtrack variability.

A notable distinction between the analyses used to identify baroclinic annular variability in the Southern and Northern Hemispheres lies in the filtering of the wave fluxes. The baroclinic annular modes are consistent with two-way feedbacks between the baroclinicity and the wave fluxes of heat by synoptic-scale waves (Thompson and Barnes 2014). In the SH, the total variance in the eddy kinetic energy is dominated by waves on synoptic scales and thus the SBAM emerges from PC analysis of the full eddy kinetic energy field. However, in the NH the total variance in the eddy kinetic energy field includes a substantial contribution from the planetary-scale waves. For this reason, the NBAM emerges most clearly from PC analysis of the eddy kinetic energy field after the variance due to planetary-scale waves has been filtered from the data.

As is the case in the SH, the northern baroclinic and barotropic annular modes (the NBAM and NAM) together account for large fractions of the variability in the cycling of energy through the NH circulation. The NBAM accounts for large fractions of the variance in 1) the conversions between available zonal-mean and eddy potential energy and 2) the eddy kinetic energy. The NAM accounts for large fractions of the variance in 1) the conversions between eddy and zonal-mean kinetic energy and 2) the zonal-mean kinetic energy.

Also like the SH, the NBAM exhibits notable periodicity on timescales of ~20-25 days. The periodicity in the NBAM is most pronounced during the summer season when it extends to the eddy fluxes of heat by synoptic eddies and also precipitation. The dynamics and implications of the periodicity in the NBAM will be examined in the companion study (Thompson and Barnes 2015).

References

Ambaum, M. H. P., and L. Novak, 2014: A nonlinear oscillator describing storm track variability. Quart. J. Roy. Meteor. Soc., 139. doi:10.1002/qj.2352.

Chang, E. K. M., and D. B. Yu, 1999: Characteristics of wave packets in the upper troposphere. Part I: Northern Hemisphere winter. J. Atmos. Sci., 56, 1708–1728.

Chang, E. K. M., and Y. Fu, 2002: Interdecadal variations in Northern Hemisphere winter storm track intensity. J. Climate, 15, 642–658.

Chang, E. K. M., 2004: Are the Northern Hemisphere winter storm tracks significantly correlated? J. Climate, 17, 4230–4244.

Dee, D. P., and Coauthors, 2011: The ERA-Interim reanalysis: Configuration and performance of the data assimilation system. Quart. J. Roy. Meteor. Soc., 137, 553–597, doi:10.1002/qj.828.

DeWeaver, E. and S. Nigam, 2000: Do Stationary Waves Drive the Zonal-Mean Jet Anomalies of the Northern Winter? J. Climate, 13, 2160–2176.

Feldstein, S. B., 2003: The dynamics of NAO teleconnection pattern growth and decay. Quarterly Journal of the Royal Meteorological Society 129:589, 901-924

Gerber, E. P., and G. K. Vallis, 2005: A Stochastic Model for the Spatial Structure of Annular Patterns of Variability and the North Atlantic Oscillation. J. Climate, 18, 2102–2118.

Hartmann, D. L. and F. Lo, 1998: Wave-driven zonal flow vacillation in the Southern Hemisphere. J. Atmos. Sci., 55, 1303–1315.

Hurrell, J. W., 1995: Decadal trends in the North Atlantic Oscillation: Regional temperatures and precipitation. Science, 269, 676–679.

Kidson, J. W., 1988: Interannual variations in the Southern Hemisphere circulation. J.

Climate, 1, 1177-1198.

Lau, N.-C., 1988: Variability of the observed midlatitude storm tracks in relation to low-frequency changes in the circulation pattern. J. Atmos. Sci., 45, 2718–2743.

Li, Y., and N.-C. Lau, 2012: Contributions of Downstream Eddy Development to the Teleconnection between ENSO and the Atmospheric Circulation over the North Atlantic. J. Climate, 25, 4993–5010.

Limpasuvan, V. and D. L. Hartmann, 2000: Wave-maintained annular modes of climate variability. J. Climate, 13, 4414–4429.

Lorenz, D. J. and D. L. Hartmann, 2001: Eddy-zonal flow feedback in the Southern Hemisphere. J. Atmos. Sci., 58, 3312–3327.

Lorenz, D. J., and D. L. Hartmann, 2003: Eddy–zonal flow feed- back in the Northern Hemisphere winter. J. Climate, 16, 1212– 1227.

Limpasuvan, V. and D. L. Hartmann, 2000: Wave-maintained annular modes of climate variability. J. Climate, 13, 4414–4429.

North, G. R., T. L. Bell, R. F. Cahalan, and F. J. Moeng, 1982: Sampling errors in the estimation of empirical orthogonal functions. Mon. Wea. Rev., 110, 699–706.

Quadrelli, R., and J. M. Wallace, 2004: A simplified linear frame- work for interpreting patterns of Northern Hemisphere wintertime climate variability. J. Climate, 17, 3728–3744.

Simmons, A. J., and B. J. Hoskins, 1978: The life cycles of some nonlinear baroclinic waves. J. Atmos. Sci., 35, 414–432.

Thompson, D. W. J., and J. M. Wallace, 2000: Annular modes in the extratropical circulation. Part I: Month-to-month variability. J. Climate, 13, 1000–1016.

Thompson, D. W. J., and E. A. Barnes, 2014: Periodic Variability in the Large-Scale

Southern Hemisphere Atmospheric Circulation. Science, 343, 641-645.

Thompson, D. W. J., and J. D. Woodworth, 2014: Barotropic and baroclinic annular variability in the Southern Hemisphere. J. Atmos. Sci., 71, 1480-1493.

Wallace, J. M., 2000: North Atlantic Oscillation/Annular Mode: Two paradigms—One phenomenon. Quart. J. Roy. Meteor. Soc., 126, 791–805.

Wallace, J. M., and D. S. Gutzler, 1981: Teleconnections in the geopotential height field during the Northern Hemisphere winter. Mon. Wea. Rev., 109, 784–812.

Wettstein, J.J., and J.M. Wallace, 2010: Observed Patterns of Month-to-Month Storm Track Variability and Their Relationship to the Background Flow. J. Atmos. Sci., 67, 1420-1437.

Table Captions

Table 1: Variance explained by the PCs considered in this study. The PCs are calculated for zonal-mean, daily-mean data between 1000-200 hPa and 20°–70°N for the fields indicated. ZKE denotes the zonal-mean kinetic energy; EKE_{WN4+} the zonal-mean eddy kinetic energy associated with zonal wavenumbers 4 and higher; Atlantic and Pacific denote data restricted to longitude bands 110°W–70°E, and 70°E–110°W, respectively; cold and warm denote data restricted to October–March and April–September, respectively. All leading PCs are well separated from the second PC as per the criterion outlined in North et al. (1982).

Table 2: Correlations between the leading PCs of the fields indicated. The PCs are described in association with Table 1. Correlations are computed between 10-day low pass filtered versions of the PC time series. Bold font indicates results that are significant at the 99% confidence level based on a two-tailed test of the *t*-statistic.

Figure Captions

Figure 1: Latitude/lag structure of the leading PCs of eddy kinetic energy (EKE) in the Southern Hemisphere (SH; left) and Northern Hemisphere (NH; right). (top) Daily-mean, zonal-mean values of the eddy fluxes of heat at 850 hPa (shading) and EKE at 300 hPa (contours) regressed onto the leading PC time series of EKE. The PC time series are derived from analysis of unfiltered EKE within 1000-200 hPa and 20°-70°. (middle and bottom) Components of the regressions in the top panels that derive from synoptic (zonal wavenumbers 4 and higher) and planetary scale (zonal wavenumbers 1-3) waves. Negative lags denote the field leads the PC time series, and vice versa. Contour intervals are $-3.5, 3.5, 10.5 \ldots$ m^2 s^{-2}.

Figure 2: Vertical structure of the northern annular mode (NAM) and northern baroclinic annular mode (NBAM) in the zonal-mean circulation. Results show daily-mean, zonal-mean values of the fields indicated regressed on standardized values of the NAM (left) and NBAM (right) indices. The NAM index is defined as the leading PC time series of NH zonal-mean zonal wind. The NBAM index is defined as the leading PC of NH synoptic-scale zonal-mean eddy kinetic energy. Results are based on daily-mean data for all calendar months. Regression coefficients are based on contemporaneous values of the data, except in the cases of $[u^*v^*]$ and $[v^*T^*]$, in which the fluxes lead the NAM and NBAM indices by 1 day. Contour intervals are $-0.5, 0.5, 1.5 \ldots$ m s^{-1} (top); $-0.5, 0.5, 1.5\times10^9$ kg s^{-1} (middle); $-3, 3, 9 \ldots$ m^2 s^{-2} (bottom). Solid and dashed contours denote clockwise and counterclockwise motion in the middle panels.

Figure 3: Latitude/lag structure of NAM and NBAM in zonal-mean kinetic energy. Results show daily-mean, zonal-mean values of the fields indicated regressed on standardized values of the NAM (left) and NBAM (right) indices as a function of latitude and lag. The momentum fluxes, zonal wind and eddy kinetic energy are shown at 300 hPa. The heat fluxes are shown at 850 hPa. Negative lags denote the field leads the base index, and vice versa. Contours are shown at −0.35, 0.35, 1.5 ... m s^{-1} (left); −3.5, 3.5, 10.5 ... m^2 s^{-2} (right).

Figure 4: Wavenumber breakdown of the latitude/lag structure of NAM and NBAM in the eddy fluxes of heat and momentum. Results show daily-mean, zonal-mean values of the fields indicated regressed on standardized values of the NAM (left) and NBAM (right) indices as a function of latitude and lag. (top) unfiltered data (reproduced from the corresponding results in Fig. 3). (middle and bottom) the components of the regressions in the top panels that are due to synoptic (zonal wavenumbers 4 and higher) and planetary scale (zonal wavenumbers 1-3) waves. Negative lags denote the field leads the base index, and vice versa. Contour interval is 4 m^2 s^{-2}.

Figure 5: Percent variance explained by the NAM (left) and NBAM (right) in vertically averaged values of the indicated fields. The time series and data are 10 day low-pass filtered to emphasize covariability on timescales longer than those associated with a typical baroclinic wave. The fields are vertically averaged between 950 and 250 hPa.

Figure 6: Horizontal structure of the NBAM in EKE at 300 hPa. Results show daily-mean eddy kinetic energy at 300 hPa regressed onto standardized values of NBAM index.

Figure 7: (a) Correlations between the NAM index and the leading PCs of the daily-mean, longitudinally-varying zonal wind. The PCs are calculated as a function of latitude. (b) Variances explained by the first and second PCs of the daily-mean, longitudinally-varying zonal wind. (c) As in (a), but for correlations between the NBAM index and the leading PCs of daily-mean, synoptic-scale eddy kinetic energy. (d) As in (b), but for the PCs of the daily-mean, synoptic-scale eddy kinetic energy. Error bars are derived from the significance test described in North et al. (1982). The PCs are calculated based on daily-mean data. The correlations are based on 10 day low-pass versions of the time series to emphasize covariability on timescale longer than those associated with a typical baroclinic wave

Figure 8: Structure of baroclinic annular variability over the North Atlantic and North Pacific sectors of the hemisphere. As in the right column of Figure 2, but for results calculated separately for the Atlantic (left; 70°W-110°E) and Pacific (right; 70°W-110°E) sectors of the hemisphere. The $NBAM_{Atlantic}$ is defined as the leading PC time series of synoptic-scale EKE in the Atlantic sector from 1000-200 hPa; the $NBAM_{Pacific}$ index as the leading PC time series of synoptic-scale EKE in the Pacific sector from 1000-200 hPa.

Figure 9: Lead/lag correlations between the $NBAM_{Pacific}$ index and $NBAM_{Atlantic}$ index. Negative lags denote the $NBAM_{Atlantic}$ index leads the $NBAM_{Pacific}$, and vice versa. The horizontal dashed line indicates the 99% significance level based on a two-tailed test of the *t*-statistic.

Figure 10: Regressions of eddy kinetic energy at 300 hPa onto the $NBAM_{Pacific}$ index as a function of lag. Stippling indicates results that exceed 99% confidence level based on a two-tailed test of the *t*-statistic.

Figure 11: As in Fig. 9, but for lead/lag correlations between the $NBAM_{Pacific}$ index and eddy kinetic energy at 300 hPa averaged over Gulf Stream extension region (see black borders indicated in Fig. 10e). Horizontal line indicates 99% significance levels based on a two-tailed test of the *t*-statistic.

Figure 12: Power spectra of the NBAM index calculated from daily-mean data for (a) all calendar days, (b) warm season days only, (c) cold season days only. Warm and cold months are defined as April–September, and October–March, respectively. See text for details of the calculation.

Figure 13: As in Figure 12, but left panels show spectra of the NBAM for the first half of the data record, and right panels show spectra for the second half of the data record.

Figure 14. Power spectra of the a) synoptic-scale eddy kinetic energy at 300 hPa, b) synoptic-scale eddy fluxes of heat at 850 hPa, and c) precipitation averaged 30° to 70°N. Results are based on warm season data. Precipitation is based on ERA-Interim (see Section 2).

Figure 15: Comparing the vertical structures of the southern and northern baroclinic annular modes. Results show daily-mean, zonal-mean values of the fields indicated regressed on standardized values of the SBAM (left) and NBAM (right) indices. Results

for the NBAM are reproduced from Fig. 2 (right column). Results for the SBAM are reproduced from TW (but based on the period of record January 1979-December 2011).

TABLE 1. Variance explained by the PCs considered in this study. The PCs are calculated for zonal-mean, daily-mean data between 1000–200 hPa and 20°–70°N for the fields indicated. ZKE denotes the zonal-mean kinetic energy; EKE_{WN4+} the zonal-mean eddy kinetic energy associated with zonal wavenumbers 4 and higher; Atlantic and Pacific denote data restricted to longitude bands 110°W–70°E, and 70°E–110°W, respectively; cold and warm denote data restricted to October–March and April–September, respectively. All leading PCs are well separated from the second PC as per the criterion outlined in North et al. (1982).

Variance explained	U (NAM)	ZKE	EKE_{WN4+} (NBAM)	$EKE^{Atlantic}_{WN4+}$	$EKE^{Pacific}_{WN4+}$	EKE^{cold}_{WN4+}	EKE^{warm}_{WN4+}
PC1	34.1	37.0	43.0	41.6	44.7	45.4	40.9
PC2	25.4	27.1	18.3	19.8	18.3	16.7	18.5

TABLE 2. Correlations between the leading PCs of the fields indicated. The PCs are described in association with Table 1. Correlations are computed between 10-day low pass filtered versions of the PC time series. Bold font indicates results that are significant at the 99% confidence level based on a two-tailed test of the t-statistic.

	PC1 $\mathrm{EKE}_{\mathrm{WN4+}}$(NBAM)	PC1 ZKE	PC1 U (NAM)
PC1 $\mathrm{EKE}_{\mathrm{WN4+}}$(NBAM)	**1**	**0.15**	**0.15**
PC1 ZKE	**0.15**	**1**	**0.85**

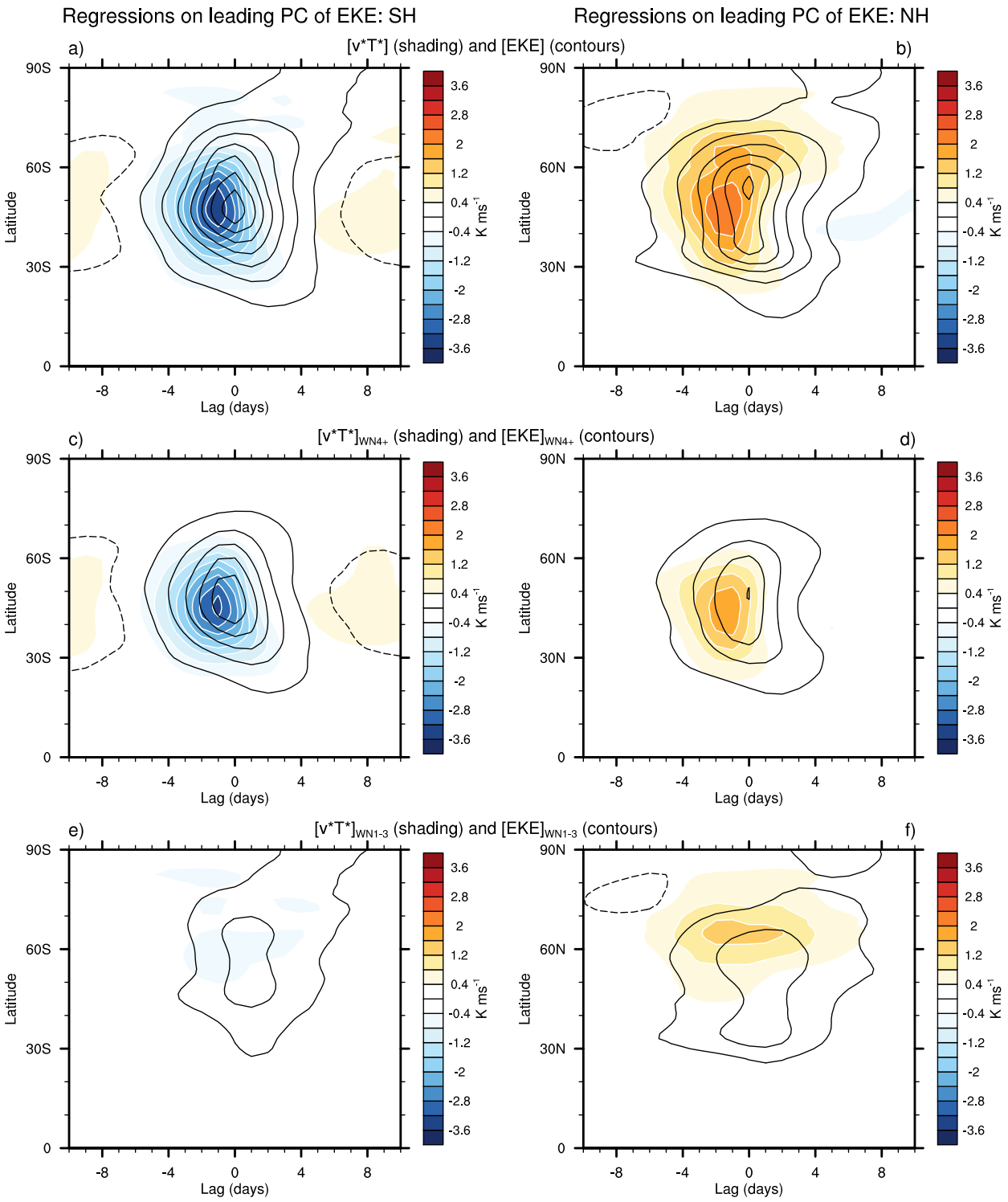

FIG. 1. Latitude/lag structure of the leading PCs of eddy kinetic energy (EKE) in the Southern Hemisphere (SH; left) and Northern Hemisphere (NH; right). (top) Daily-mean, zonal-mean values of the eddy fluxes of heat at 850 hPa (shading) and EKE at 300 hPa (contours) regressed onto the leading PC time series of EKE. The PC time series are derived from analysis of unfiltered EKE within 1000-200 hPa and 20°–70°. (middle and bottom) Components of the regressions in the top panels that derive from synoptic (zonal wavenumbers 4 and higher) and planetary scale (zonal wavenumbers 1-3) waves. Negative lags denote the field leads the PC time series, and vice versa. Contour intervals are −3.5, 3.5, 10.5 ... $m^2\ s^{-2}$.

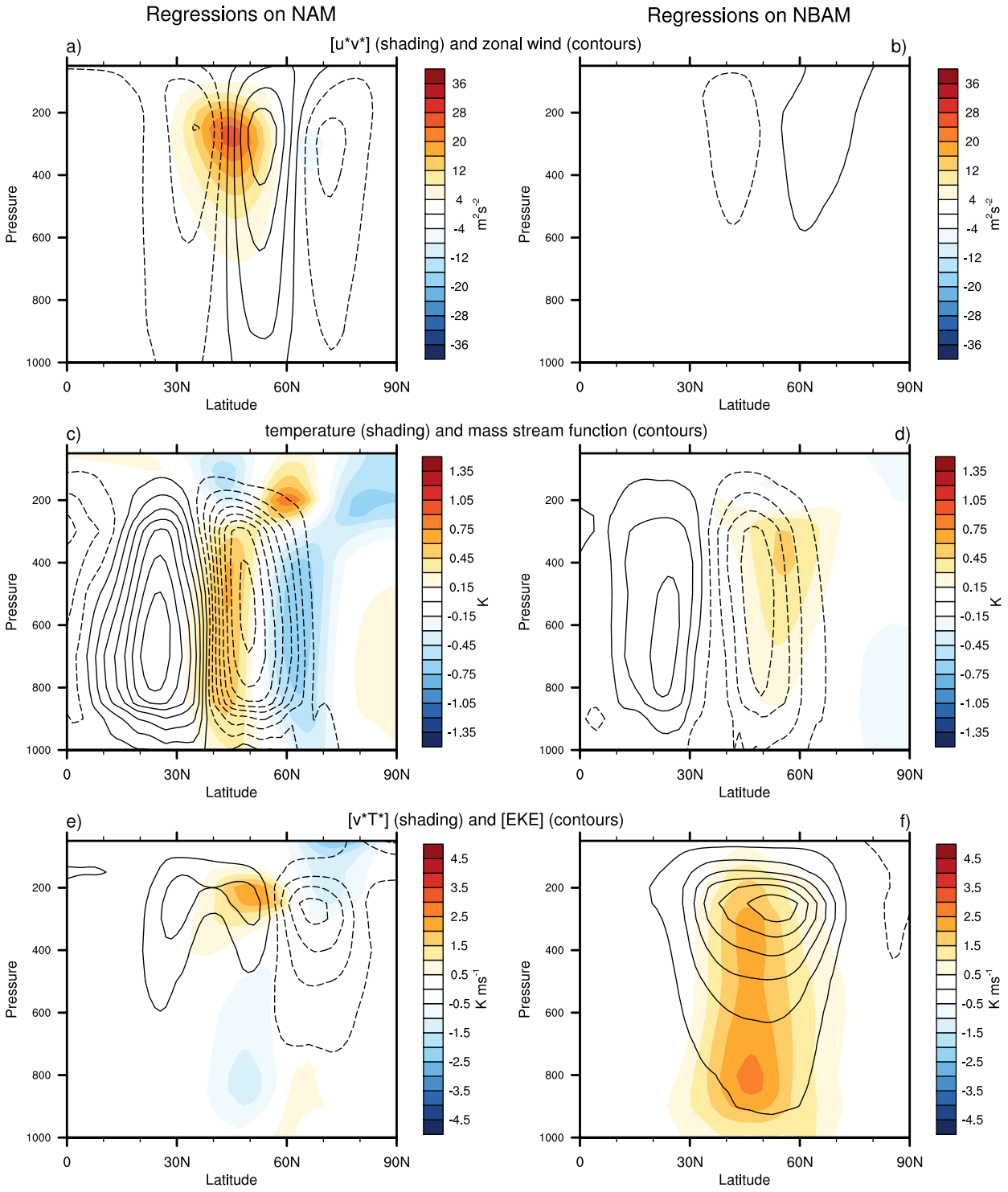

FIG. 2. Vertical structure of the northern annular mode (NAM) and northern baroclinic annular mode (NBAM) in the zonal-mean circulation. Results show daily-mean, zonal-mean values of the fields indicated regressed on standardized values of the NAM (left) and NBAM (right) indices. The NAM index is defined as the leading PC time series of NH zonal-mean zonal wind. The NBAM index is defined as the leading PC of NH synoptic-scale zonal-mean eddy kinetic energy. Results are based on daily-mean data for all calendar months. Regression coefficients are based on contemporaneous values of the data, except in the cases of $[u^*v^*]$ and $[v^*T^*]$, in which the fluxes lead the NAM and NBAM indices by 1 day. Contour intervals are -0.5, 0.5, 1.5 ... m s^{-1} (top); -0.5, 0.5, 1.5×10^9 kg s^{-1} (middle); -3, 3, 9 ... m^2 s^{-2} (bottom). Solid and dashed contours denote clockwise and counterclockwise motion in the middle panels.

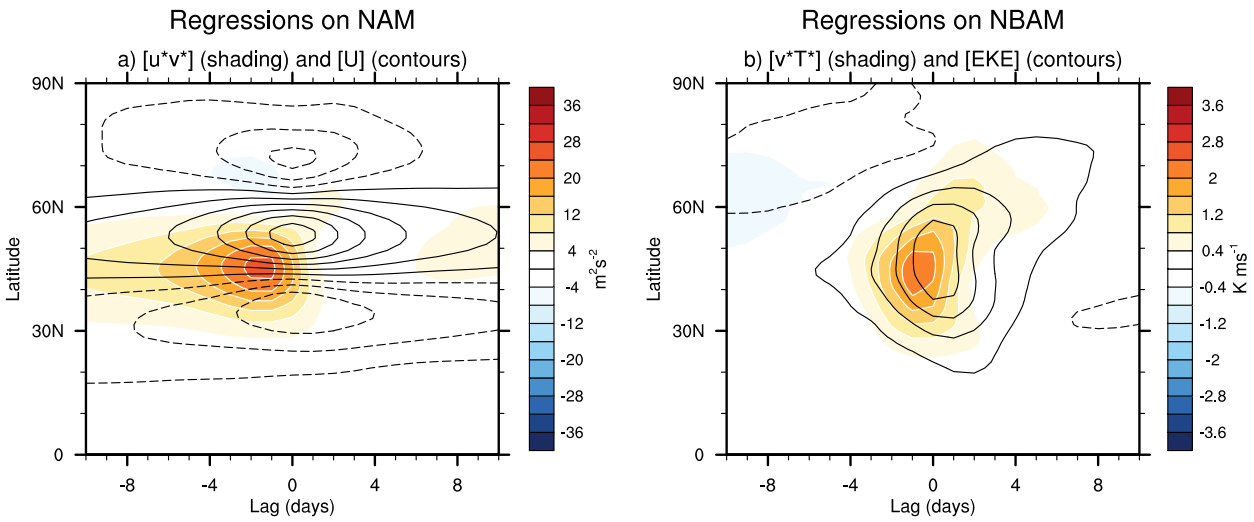

FIG. 3. Latitude/lag structure of NAM and NBAM in zonal-mean kinetic energy. Results show daily-mean, zonal-mean values of the fields indicated regressed on standardized values of the NAM (left) and NBAM (right) indices as a function of latitude and lag. The momentum fluxes, zonal wind and eddy kinetic energy are shown at 300 hPa. The heat fluxes are shown at 850 hPa. Negative lags denote the field leads the base index, and vice versa. Contours are shown at -0.35, 0.35, 1.5 ... m s^{-1} (left); -3.5, 3.5, 10.5 ... m^2 s^{-2} (right).

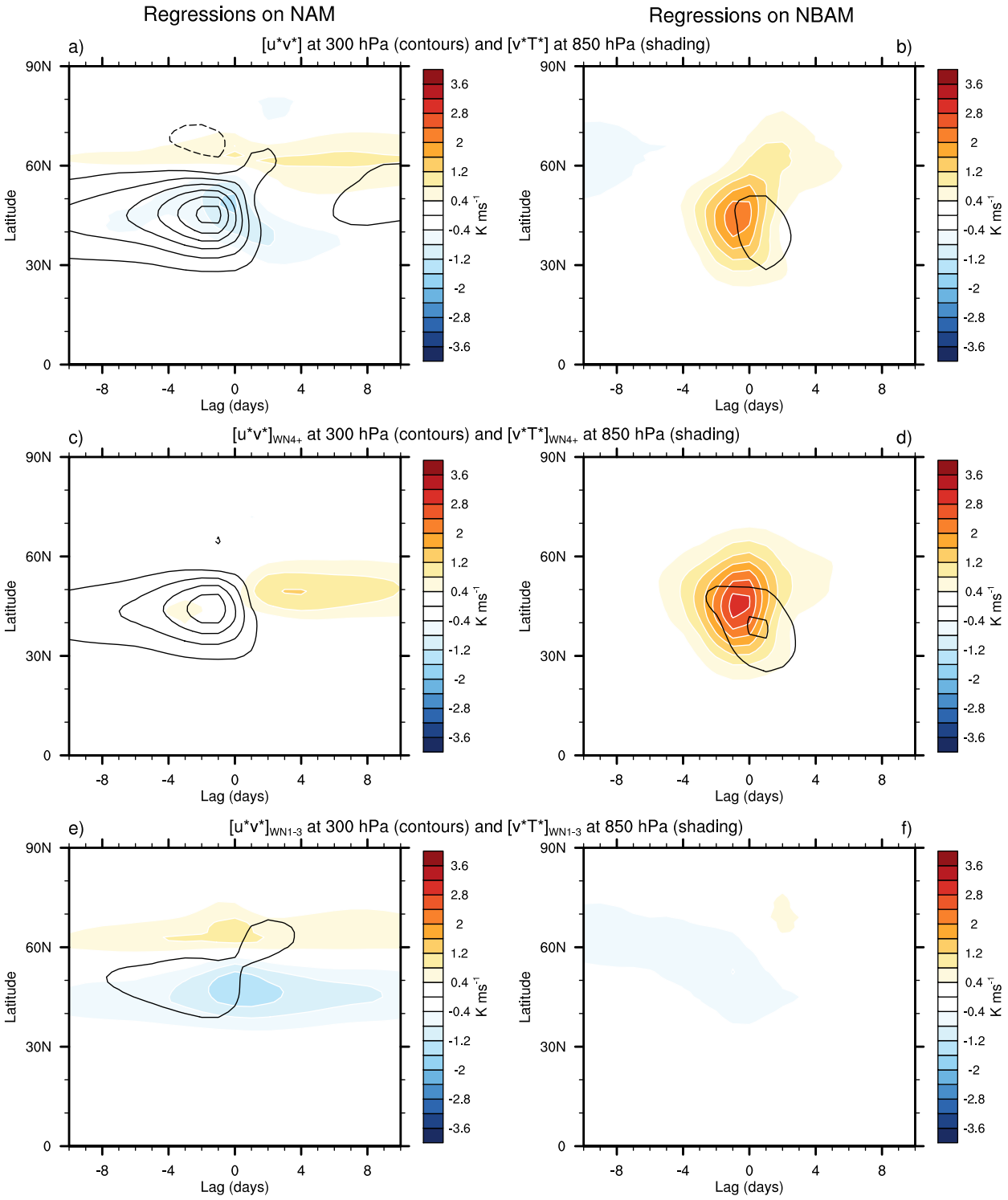

FIG. 4. Wavenumber breakdown of the latitude/lag structure of NAM and NBAM in the eddy fluxes of heat and momentum. Results show daily-mean, zonal-mean values of the fields indicated regressed on standardized values of the NAM (left) and NBAM (right) indices as a function of latitude and lag. (top) unfiltered data (reproduced from the corresponding results in Fig. 3). (middle and bottom) the components of the regressions in the top panels that are due to synoptic (zonal wavenumbers 4 and higher) and planetary scale (zonal wavenumbers 1-3) waves. Negative lags denote the field leads the base index, and vice versa. Contour interval is 4 m^2 s^{-2}.

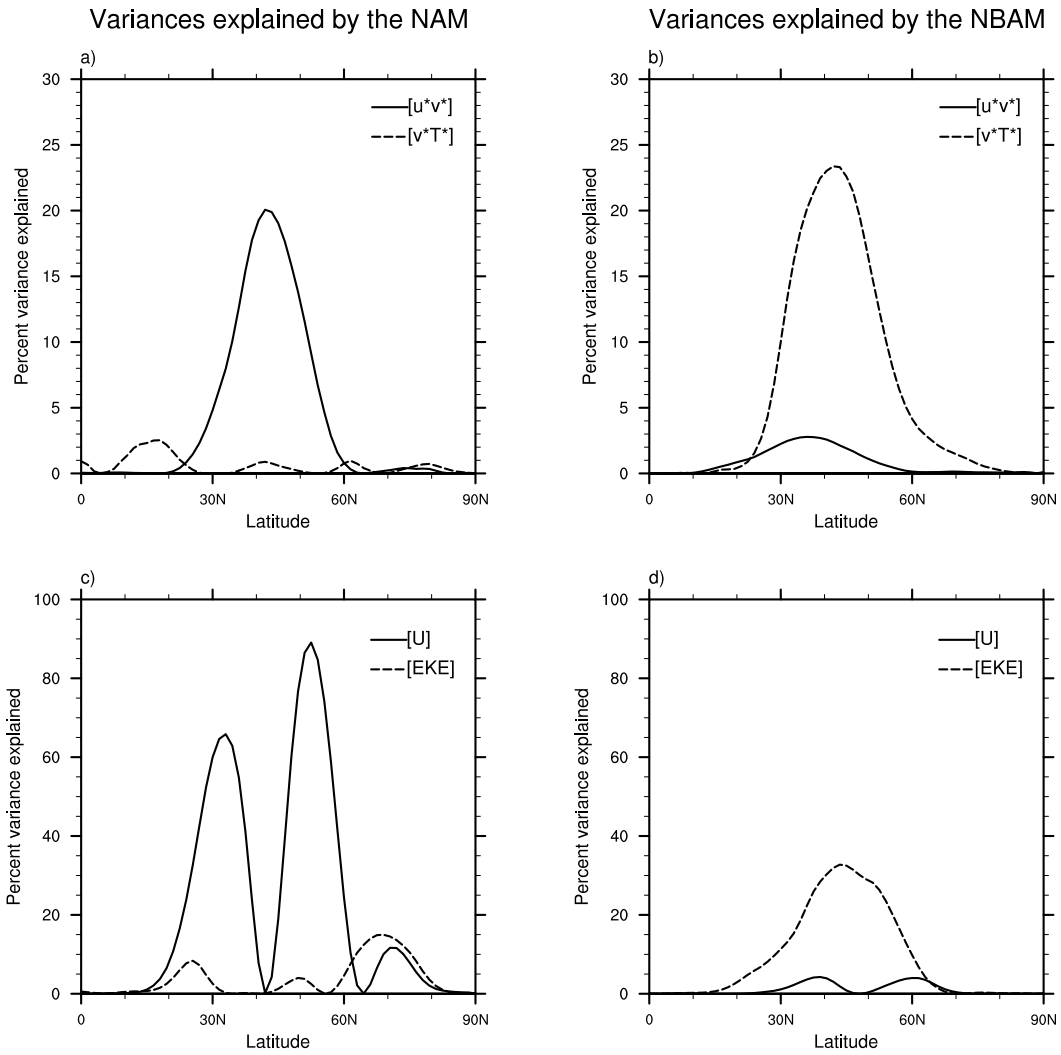

FIG. 5. Percent variance explained by the NAM (left) and NBAM (right) in vertically averaged values of the indicated fields. The time series and data are 10 day low-pass filtered to emphasize covariability on timescales longer than those associated with a typical baroclinic wave. The fields are vertically averaged between 950 and 250 hPa.

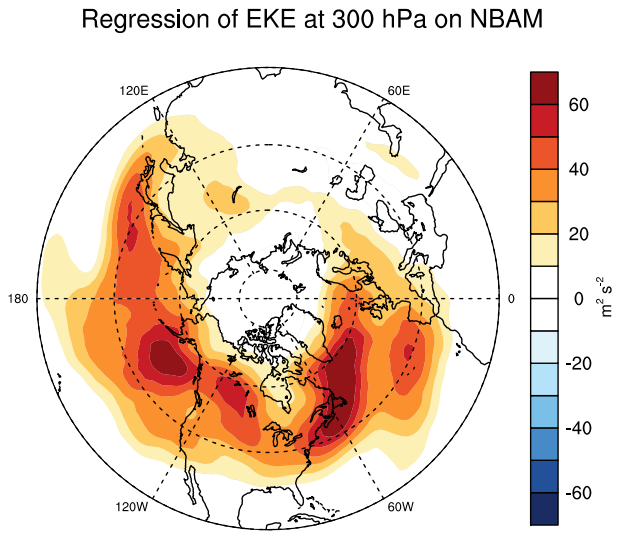

FIG. 6. Horizontal structure of the NBAM in EKE at 300 hPa. Results show daily-mean eddy kinetic energy at 300 hPa regressed onto standardized values of NBAM index.

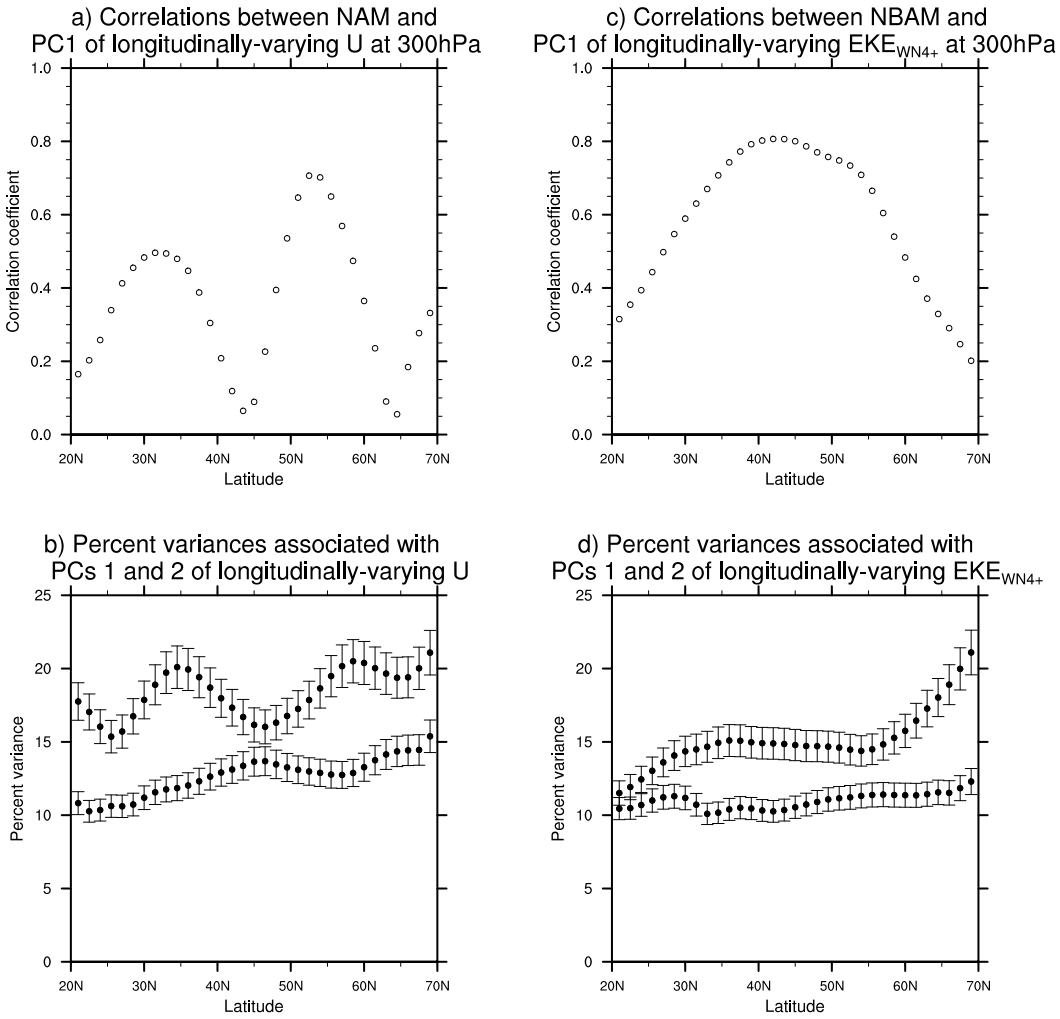

FIG. 7. (a) Correlations between the NAM index and the leading PCs of the daily-mean, longitudinally-varying zonal wind. The PCs are calculated as a function of latitude. (b) Variances explained by the first and second PCs of the daily-mean, longitudinally-varying zonal wind. (c) As in (a), but for correlations between the NBAM index and the leading PCs of daily-mean, synoptic-scale eddy kinetic energy. (d) As in (b), but for the PCs of the daily-mean, synoptic-scale eddy kinetic energy. Error bars are derived from the significance test described in North et al. (1982). The PCs are calculated based on daily-mean data. The correlations are based on 10 day low-pass versions of the time series to emphasize covariability on timescale longer than those associated with a typical baroclinic wave.

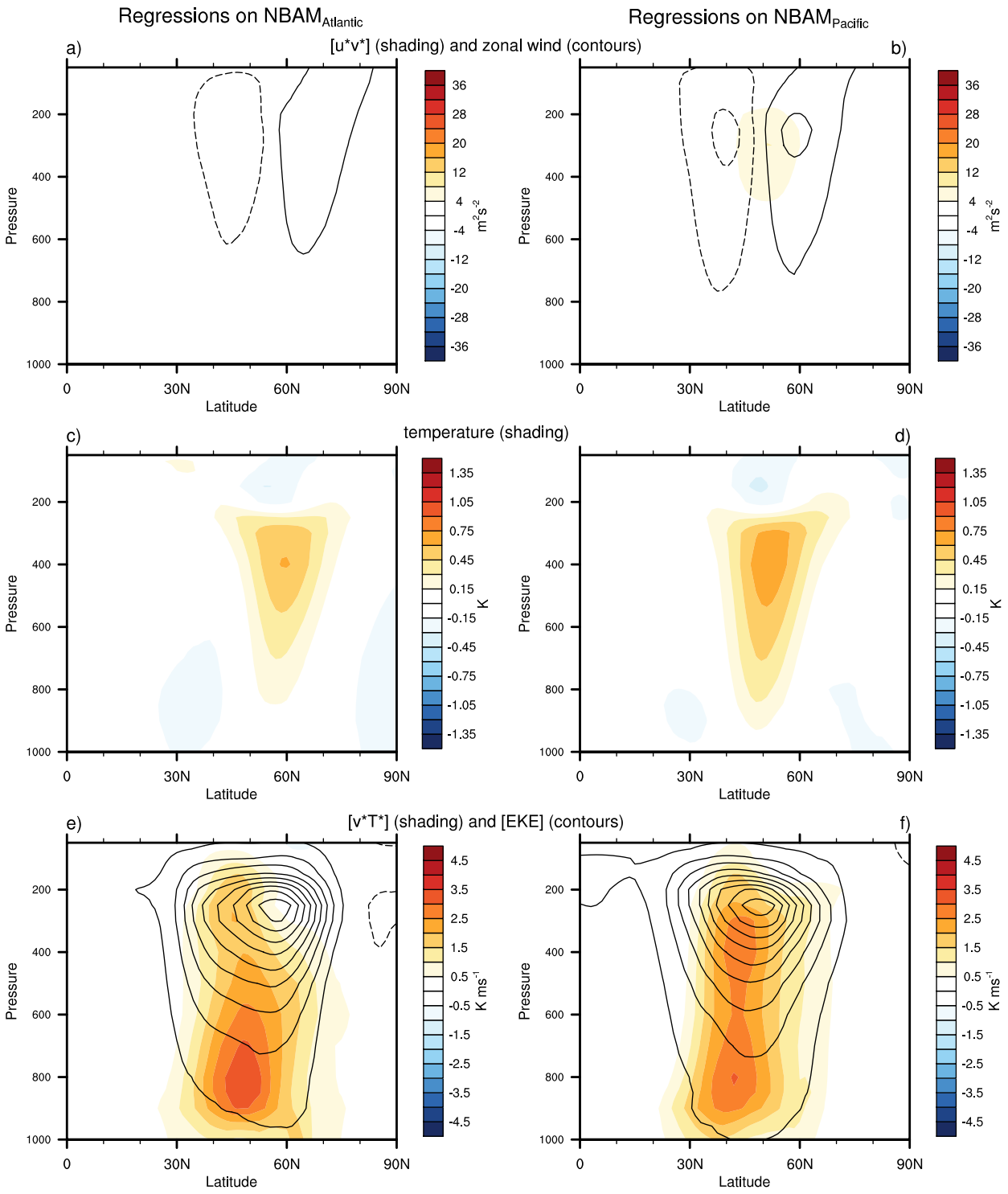

FIG. 8. Structure of baroclinic annular variability over the North Atlantic and North Pacific sectors of the hemisphere. As in the right column of Figure 2, but for results calculated separately for the Atlantic (left; 70°W–110°E) and Pacific (right; 70°W–110°E) sectors of the hemisphere. The NBAM$_{\text{Atlantic}}$ is defined as the leading PC time series of synoptic-scale EKE in the Atlantic sector from 1000-200 hPa; the NBAM$_{\text{Pacific}}$ index as the leading PC time series of synoptic-scale EKE in the Pacific sector from 1000–200 hPa.

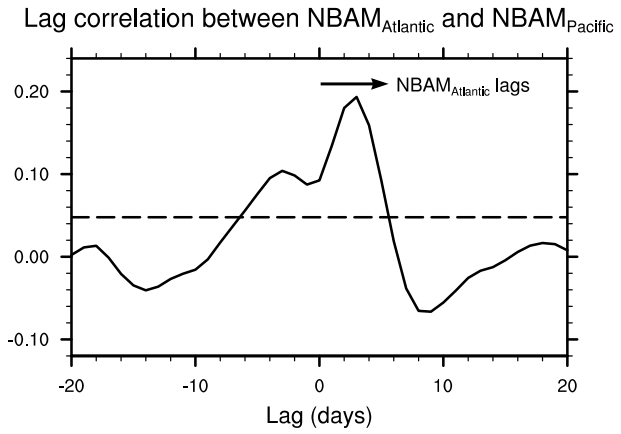

FIG. 9. Lead/lag correlations between the $\mathrm{NBAM_{Pacific}}$ index and $\mathrm{NBAM_{Atlantic}}$ index. Negative lags denote the $\mathrm{NBAM_{Atlantic}}$ index leading the $\mathrm{NBAM_{Pacific}}$, and vice versa. The horizontal dashed line indicates the 99% significance level based on a two-tailed test of the t-statistic.

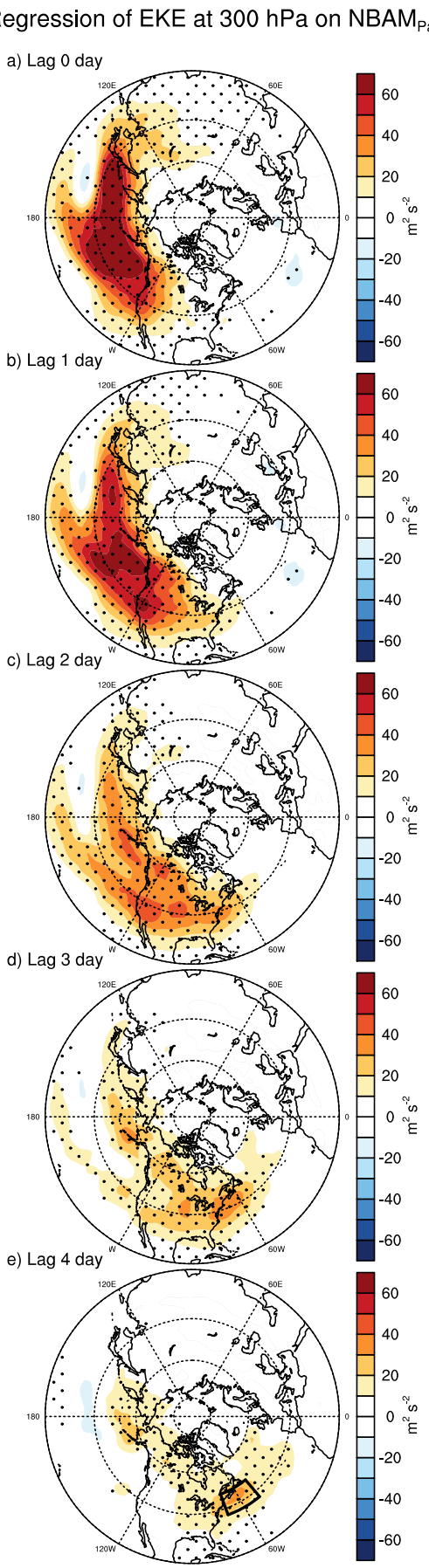

FIG. 10. Regressions of eddy kinetic energy at 300 hPa onto the NBAM$_{\text{Pacific}}$ index as a function of lag. Stippling indicates results that exceed 99% confidence level based on a two-tailed test of the t-statistic.

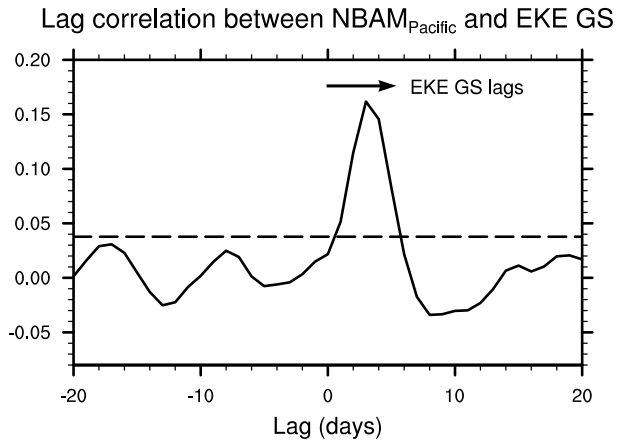

FIG. 11. As in Fig. 9, but for lead/lag correlations between the NBAMPacific index and eddy kinetic energy at 300 hPa averaged over Gulf Stream extension region (GS; see black borders indicated in Fig. 10e). Horizontal line indicates 99% significance levels based on a two-tailed test of the t-statistic.

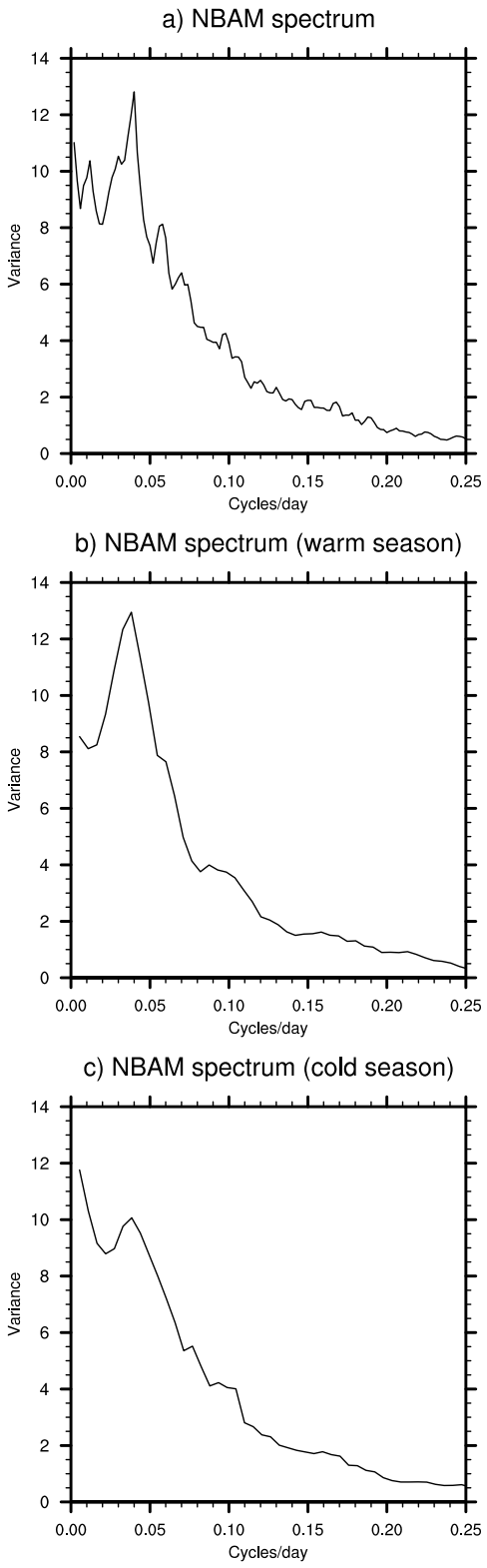

FIG. 12. Power spectra of the NBAM index calculated from daily-mean data for (a) all calendar days, (b) warm season days only, (c) cold season days only. Warm and cold months are defined as AprilSeptember, and OctoberMarch, respectively. See text for details of the calculation.

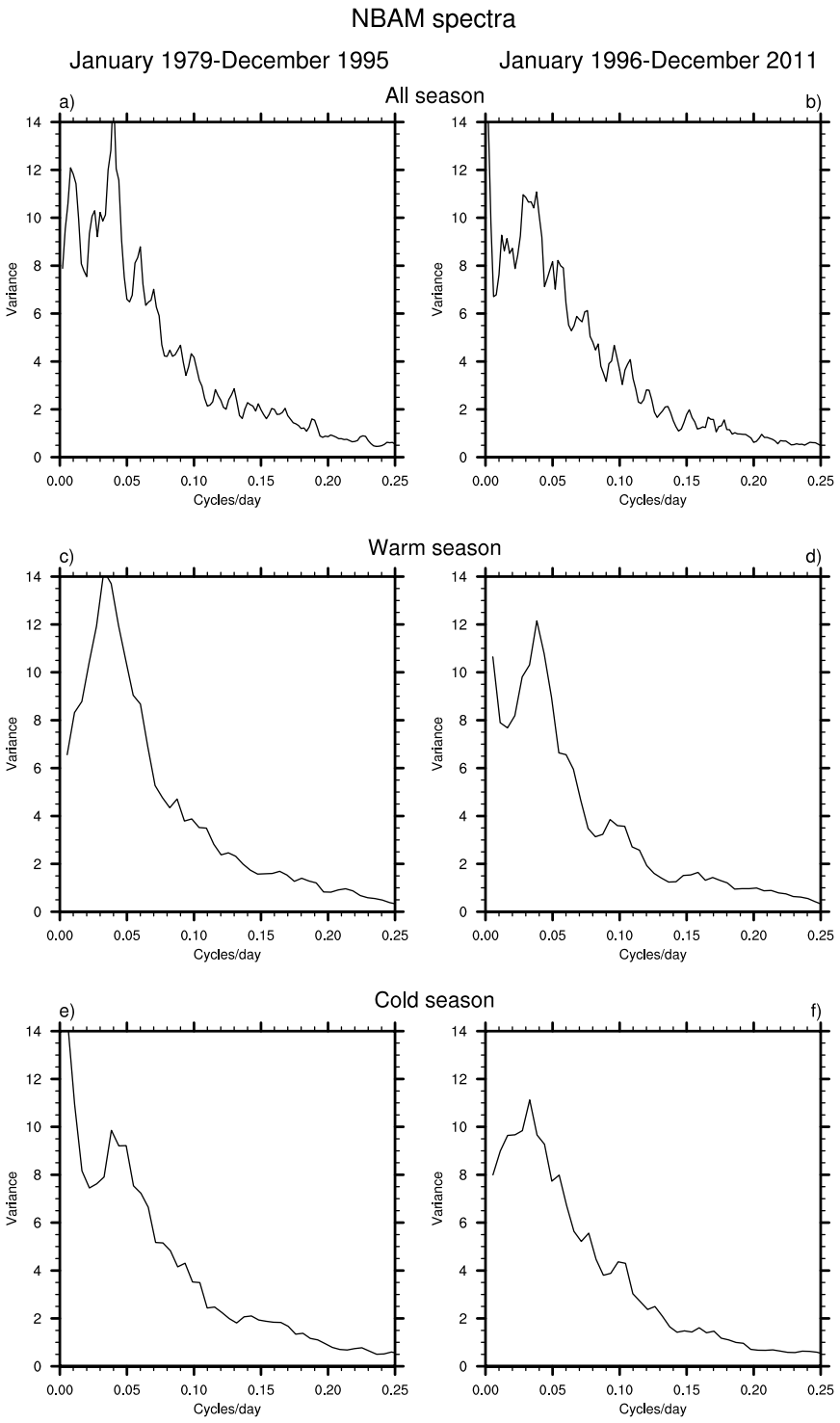

FIG. 13. As in Figure 12, but left panels show spectra of the NBAM for the first half of the data record, and right panels show spectra for the second half of the data record.

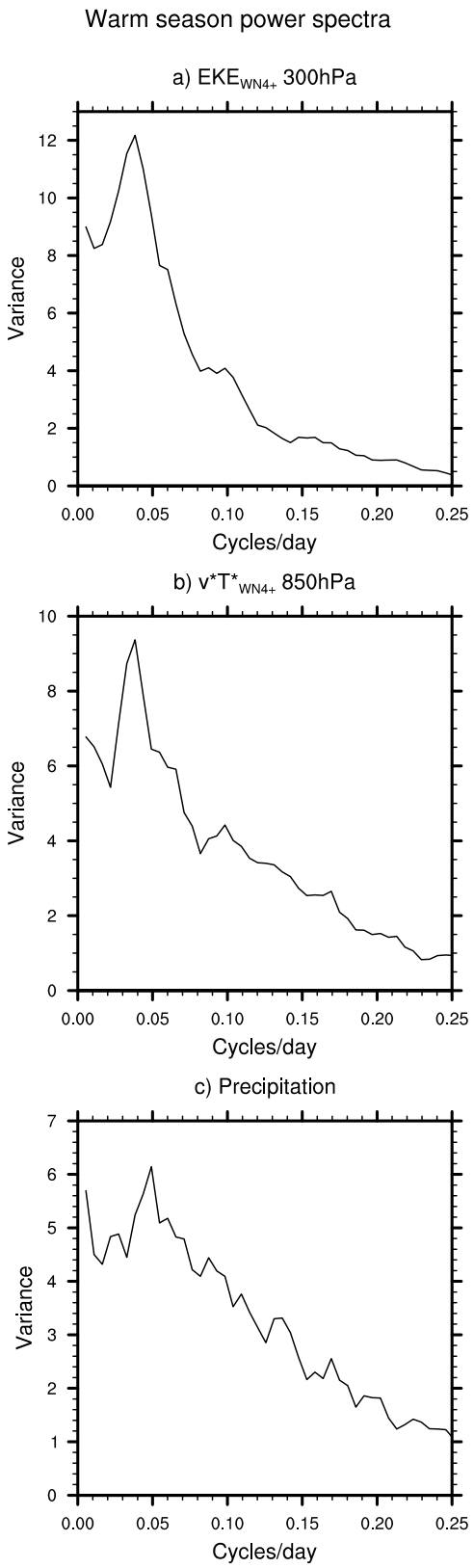

FIG. 14. Power spectra of the a) synoptic-scale eddy kinetic energy at 300 hPa, b) synoptic-scale eddy fluxes of heat at 850 hPa, and c) precipitation averaged 30° to 70°N. Results are based on warm season data. Precipitation is based on ERA-Interim (see Section 2).

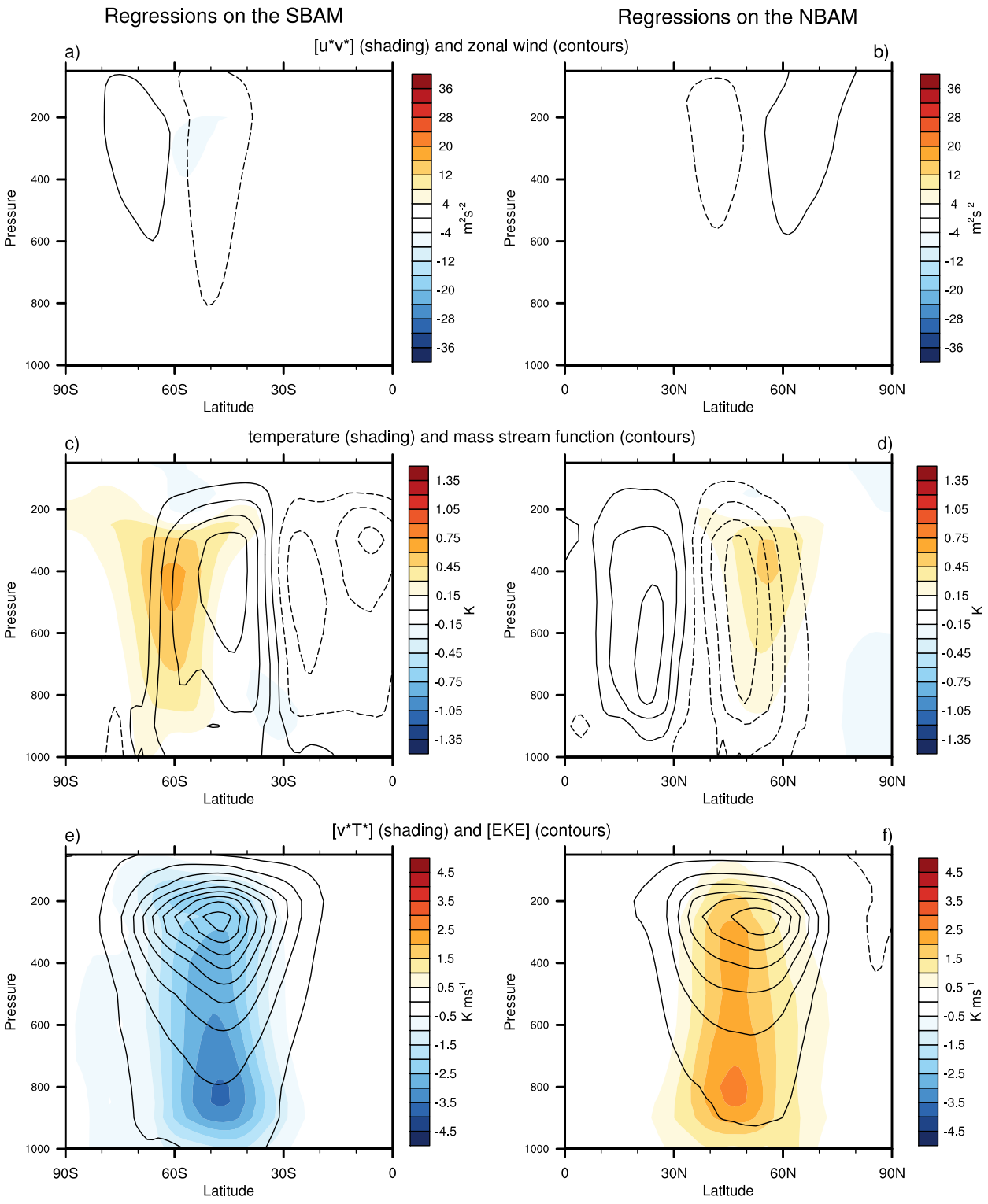

FIG. 15. Comparing the vertical structures of the southern and northern baroclinic annular modes. Results show daily-mean, zonal-mean values of the fields indicated regressed on standardized values of the SBAM (left) and NBAM (right) indices. Results for the NBAM are reproduced from Fig. 2 (right column). Results for the SBAM are reproduced from TW (but based on the period of record January 1979–December 2011).